Multineutron transfer in ^{58}Ni+^{124}Sn collisions at sub-barrier energies

C. L. Jiang, K. E. Rehm, H. Esbensen, D. J. Blumenthal, B. Crowell, J. Gehring, B. Glagola, J. P. Schiffer, and A. H. Wuosmaa
Physics Division, Argonne National Laboratory, Argonne, Illinois 60439
(Received 10 December 1997)

Cross sections for multineutron transfer reactions in ^{58}Ni+^{124}Sn collisions have been measured with good particle identification at four energies around the Coulomb barrier. The angle- and energy-integrated multineutron transfer cross sections exhibit an exponential falloff with increasing number of transferred neutrons. The elastic scattering and one-nucleon transfer reaction data can be reproduced well by coupled-channels calculations and distorted-wave Born approximation calculations, respectively, using the same optical potential. The transfer probabilities for each transfer channel, plotted as a function of the distance of closest approach, fall on a common exponential curve; the slopes of these exponential falloff curves are discussed. [S0556-2813(98)04105-3]

PACS number(s): 25.70.Hi, 25.70.Bc

I. INTRODUCTION

Heavy ion induced fusion reactions have been used extensively for studies of neutron-deficient nuclei, covering the range from the valley of stability to the proton drip line. Because of the curvature of the valley of stability in the N-Z plane, fusion reactions cannot be used to produce neutron-rich nuclei. Multineutron transfer reactions [e.g., the (^{18}O,^{16}O) reaction] on a neutron-rich target, on the other hand, can produce nuclei on the neutron-rich side of the valley of stability. Q-value restrictions limit these reactions, however, mainly to two-neutron transfer processes. Complex multinucleon transfer reactions have recently been discussed as a way to produce exotic nuclei which are not accessible by other processes [1]. The possibility of using unstable ion beams in these reactions strongly reduces the Q-value limitations as shown, e.g., in recent calculations for the systems ^{118,136,154}Xe+^{208}Pb [2]. The calculations for ^{154}Xe beams suggest that neutron-rich isotopes of polonium and mercury far away from the valley of stability can be produced. While these neutron-rich beams are not yet available for experiments, we can test the predictions of the calculations in multineutron transfer reactions with stable beams.

The transfer of many nucleons of the same kind has been studied in several systems. The transfers of up to six protons in the system ^{144}Sm+^{208}Pb [3] and of up to six neutrons in the systems ^{58}Ni+^{100}Mo [4] and ^{40}Ca+^{124}Sn [5] have been observed. Calculations using a recently developed code [6] reproduce the general features observed in the system ^{40}Ca +^{124}Sn [5], but they cannot describe the strength of the two-proton stripping and pick-up reactions in the system ^{48}Ca +^{124}Sn [7] measured at an energy above the barrier.

In this paper we report the results of a study of multinucleon transfer reactions at energies around the Coulomb barrier for the system ^{58}Ni+^{124}Sn. Of particular interest was the energy dependence of multineutron transfer reactions and a comparison of the highest-energy result with the prediction of Ref. [6]. This system was chosen since other reaction channels, including fusion evaporation [8], fusion-fission [9], neutron transfer [10–12], and deep-inelastic scatterings [13] have been studied for this system previously. Another interesting question relates to the possibility that all these data can be described in a consistent way by coupled-channels calculations. This topic will be discussed in the following paper [14].

The paper is organized as follows. In Sec. II we describe the experimental setup. In Sec. III we give a discussion of our experimental results followed by a short summary in Sec. IV.

II. EXPERIMENTAL DETAIL

The experiments were carried out at the Argonne National Laboratory's ATLAS facility with a ^{124}Sn beam bombarding a ^{58}Ni target. The ^{124}Sn ions were accelerated in the superconducting linac to energies of 512.0, 500.8, 489.6, and 480.3 MeV, respectively. Typical beam intensities were about 1 pnA. The target consisted of a highly enriched ($>$99.8%) self-supporting ^{58}Ni foil with thicknesses of 334 μg/cm^2 (at 512.0 and 500.8 MeV) and 404 μg/cm^2 (at 489.6 and 480.3 MeV). The isotopic abundances of heavier Ni isotopes in the target were 0.090, 0.005, 0.008, and 0.020 % for $A=60$, 61, 62, and 64, respectively.

The outgoing particles were momentum analyzed in an Enge split-pole spectrograph and detected in a hybrid focal-plane detector which measured the position X along the focal plane, the time-of-flight T, the nuclear charge Z, the total energy E, as well as the range R in the counter gas [15]. From these measured quantities the nuclear charge Z, the mass M, the charge state q, as well as the Q value of the reaction can be obtained. The Z and M resolutions were $Z/\Delta Z=70$ and $A/\Delta A=150$.

Angular distributions of Ni-like particles were measured at angles $\theta_{\rm lab}=10°-50°$ in steps of 5°, which correspond to $\theta_{\rm c.m.}=100°-160°$ in the center-of-mass system. At low energies this corresponds to the most interesting angle region, because most of the transfer reaction products are concentrated in the backward angle region. Sn-like particles were measured at only the most forward angles (10°–25°). Due to the large dynamic range of the split-pole spectrograph, up to 7 and 5 charge states for Sn- and Ni-like particles, respectively, could be detected simultaneously in the focal plane

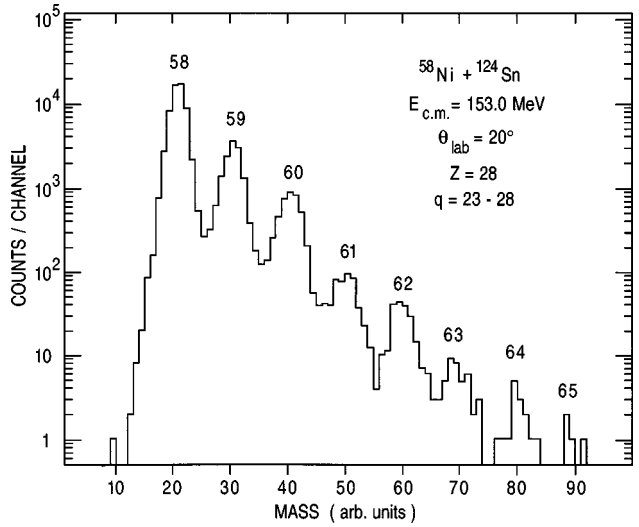

FIG. 1. Mass spectrum for $Z=28$ isotopes measured at $E_{\mathrm{c.m.}}=153.0$ MeV, $\theta_{\mathrm{lab}}=20°$, and integrated over the charge states $q=23$–26 in the system ^{58}Ni+^{124}Sn.

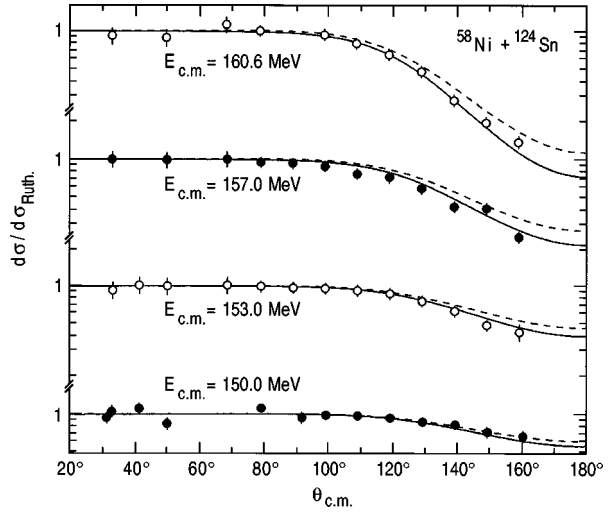

FIG. 2. Angular distributions for elastic scattering and inelastic scattering at four incident energies for the system ^{58}Ni+^{124}Sn. Solid lines are coupled channels calculations using potential V_b. Dotted lines are obtained with potential V_a.

detector with a single magnetic field setting of the spectrograph. This covered more than 60 or 80 % of the total charge-state distributions for the Sn- and Ni-like particles. A Gaussian fit to the charge state distribution was used to correct for the undetected yields.

The Q value for a given reaction product was determined from the measured position signal. The Q-value resolution was limited mostly by the difference in the stopping powers for Sn- and Ni-like particles in the target, and by the inhomogeneity and the energy-loss straggling in the target. This resolution was 3–4 MeV which is not sufficient to separate transitions to individual levels. With the large dynamic range of the spectrograph the quasielastic energy spectra of Ni-like particles could be measured simultaneously with a single magnetic field setting. The energy loss of ^{124}Sn in the target was 16–20 MeV, corresponding to a range in center-of-mass energy $E_{\mathrm{c.m.}}$ of 5–6.4 MeV. The resulting four center-of-mass energies calculated for the center of the target are 160.6, 157.0, 153.0, and 150.0 MeV.

Two monitor detectors were mounted on either side of the beam and were used to normalize the measured angular distributions. Absolute cross sections were obtained by normalizing the ^{124}Sn scattering angular distributions at the most forward angles to the corresponding Rutherford cross sections. This normalization introduced an uncertainty of about 5% and contributed to the total uncertainty in the absolute cross sections.

A mass spectrum for Ni-like particles, $Z=28$, summed over the charge states $q=23$–26, measured at $E_{\mathrm{c.m.}}=153.0$ MeV and $\theta_{\mathrm{lab}}=20°$ is shown in Fig. 1. Ni isotopes ranging from $A=58$–65, i.e., up to seven transferred neutrons, are observed. As discussed in Ref. [4] the contributions from target contaminations of other Ni isotopes to these multineutron transfer reactions can be neglected.

III. EXPERIMENTAL RESULTS

A. Elastic scattering

The measured angular distributions for elastic scattering including inelastic excitations up to about 4 MeV, relative to Rutherfold scattering are shown in Fig. 2 for the four incident energies. These angular distributions fall off smoothly from the Rutherford cross section at backward angles, with a steeper falloff at higher incident energies. Coupled-channels calculations have been performed with the code PTOLEMY [16], including the first excited 2^+ states of ^{58}Ni and ^{124}Sn. The $B(E2)$ values were taken from the literature [17], and are summarized in Table I. As shown in Ref. [12], these two states give the dominant contributions for inelastic scattering at energies around the Coulomb barrier. The optical potential used previously [4] for ^{58}Ni+^{100}Mo already gives a rather good description of the angular distributions as shown by the dotted curves in Fig. 2. A small increase of the two radius parameters r_0 and r_{0i} improves the agreement as shown by solid lines in Fig. 2. The optical potential parameters are also given in Table I. The same parameters have been used in the distorted-wave Born approximation (DWBA) calculations for transfer reactions which are discussed in the next subsection. It should be noted that from the real part of the ion-ion potential one calculates a Coulomb barrier of 160.2 MeV, less than the highest energy used in this experiment. This value is also less than the barrier $V_B=167.1$ MeV calculated from the fusion systematics by Vaz *et al.* [18].

B. Angular distributions for transfer reactions

At these low incident energies pure neutron transfer reactions are the dominant processes. Cross sections for proton

TABLE I. $B(E2)$ values and optical potentials used in the coupled-channels calculations described in the text.

Nucleus	E_{ex}(MeV)	$B(E2)(e^2b^2)$
^{58}Ni	1.454	0.070
^{124}Sn	1.132	0.166

System	V (MeV)	W (MeV)	r_0 (fm)	a_0 (fm)	r_{i0} (fm)	a_{i0} (fm)
V_a: ^{58}Ni+^{100}Mo	78.7	40.0	1.19	0.63	1.21	0.61
V_b: ^{58}Ni+^{124}Sn	78.7	40.0	1.20	0.63	1.22	0.61

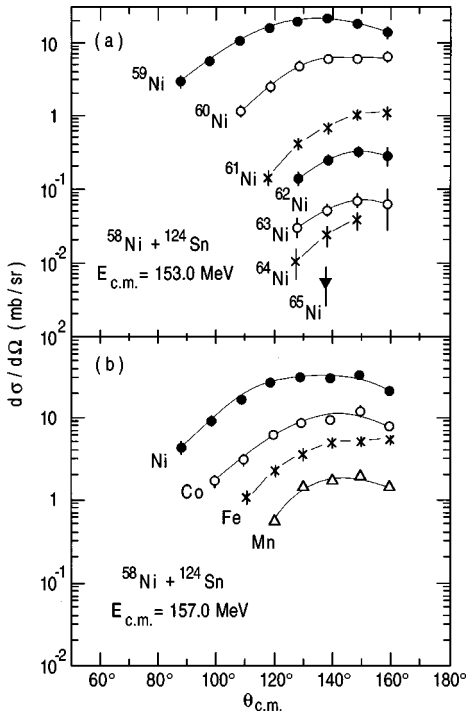

FIG. 3. Angular distributions for transfer reaction channels in the system ^{58}Ni+^{124}Sn. (a) neutron pickup channels at $E_{\mathrm{c.m.}}=153.0$ MeV. (b) proton stripping channels at $E_{\mathrm{c.m.}}=157.0$ MeV. The solid lines serve to guide the eye.

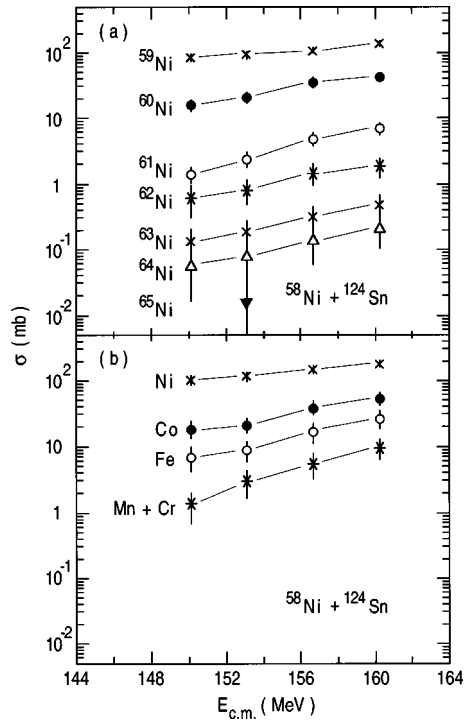

FIG. 4. Energy dependence of the angle- and excitation energy-integrated cross sections in the system ^{58}Ni+^{124}Sn. The solid lines serve to guide the eye.

transfer reactions are considerable smaller. These results are different from those obtained in the two recent studies of ^{40}Ca+^{124}Sn [5] and ^{48}Ca+^{124}Sn [7], where significant cross sections for the (yp-xn) channels were observed. The latter measurements, however, were performed at energies above the Coulomb barrier where a considerable overlap of the two nuclei can occur in central collisions.

Typical energy-integrated angular distributions are shown in Fig. 3. Angular distributions for pure neutron-pickup channels at $E_{\mathrm{c.m.}}=153.0$ MeV are shown in Fig. 3(a), while the angular distributions integrated over all Ni, Co, Fe, and Mn isotopes at $E_{\mathrm{c.m.}}=157.0$ MeV are shown in Fig. 3(b). The solid lines serve to guide the eye. At the highest energies, these angular distributions are bell shaped with a maximum that shifts to more backward angles with increasing number of transferred nucleons.

The energy dependence of the angle-integrated cross sections is shown in Fig. 4 with the cross sections tabulated in Table II. The angular distributions were extrapolated towards smaller angles using the exponential falloff property of transfer probabilities (see discussion below). The uncertainties from the extrapolation process are included in the error of the integrated cross sections. The yields are clearly dominated by neutron-transfer reactions, which at the lowest energy are about four times stronger than all the charge-transfer processes.

The results of DWBA calculations for one-neutron pickup and one-proton stripping reactions performed with the PTOLEMY [16] code are compared with the measured data at four energies in Fig. 5. The configurations for the outgoing channels taken into account in the calculations are ^{59}Ni(0.0,3/2$^-$)+^{123}Sn(0.150,1/2$^+$) and ^{57}Co(1.378,3/2$^-$)+^{125}Sb(0.700,1/2$^+$), respectively, with the optical potential parameters given in Table I. Earlier studies for the system ^{58}Ni+^{208}Pb [19] have shown that the shape of the angular distributions does not depend much on the detailed configurations used in the calculations. The calculations have been normalized to the experimental data with energy-independent normalization constants, which are different for one-neutron pickup and one-proton stripping. One can observe that these simple DWBA calculations reproduce the general trends of the measured angular distributions for one-nucleon transfer reactions at all four beam energies.

For an overall description of the experimental data we have converted the angular distributions into transfer probabilities and plotted them as a function of the distance of closest approach D. The transfer probability P_{tr} is defined as the ratio of the transfer cross section to the corresponding Rutherford cross section [20]

$$P_{\mathrm{tr}}=\frac{d\sigma_{\mathrm{tr}}}{d\sigma_{\mathrm{Ruth}}}, \tag{1}$$

and the distance of closest approach D is calculated assuming a pure Coulomb trajectory as

$$D=\frac{Z_1Z_2e^2}{2E_{\mathrm{c.m.}}}\left(1+\frac{1}{\sin(\theta_{\mathrm{c.m.}}/2)}\right). \tag{2}$$

Here $\theta_{\mathrm{c.m.}}$ is the outgoing center-of-mass angle. Figure 6 shows plots of $P_{\mathrm{tr}}/\sin(\theta_{\mathrm{c.m.}}/2)$ as a function of D for one- to six-neutron pickup, and for one- and two-proton stripping reactions. In this representation all data points measured at the four different incident energies fall on the same curve. Moreover, beyond the strong absorption region $D\sim13.8$ fm

TABLE II. Integrated cross sections for transfer reactions (in mb) for the system ^{58}Ni+^{124}Sn. For comparison the data for the system ^{58}Ni+^{100}Mo [4] are also included.

Channel	$E_{c.m.}$(MeV)=160.6	157.0	153.0	150.0	137.5 ^{58}Ni+^{100}Mo
^{59}Ni	130.7±9.9	104.9±8.4	88.9±9.8	80.8±10.5	86.1±8.6
^{60}Ni	39.5±4.3	32.7±3.9	20.2±2.2	15.3±2.3	28.2±4.2
^{61}Ni	6.8±0.9	4.8±0.6	2.3±0.4	1.4±0.3	4.8±1.0
^{62}Ni	1.8±0.5	1.4±0.2	0.80±0.12	0.61±0.24	1.3±0.4
^{63}Ni	0.47±0.14	0.30±0.07	0.18±0.05	0.13±0.06	0.40±0.16
^{64}Ni	0.20±0.08	0.13±0.04	0.079±0.032	0.055±0.027	0.14±0.07
^{65}Ni			0.015±0.008		
^{57}Co	36.2±6.5	24.7±4.9	17.4±3.8	15.8±3.7	21.4±6.0
^{56}Fe		8.5±2.8	5.7±2.1	4.6±1.8	
Ni total	179.4±15.8	144.3±13.2	112.5±12.6	98.3±13.4	121.0±14.5
Co total	51.5±9.3	38.7±7.7	21.4±4.6	18.8±4.4	25.3±6.3
Fe total	26.5±8.0	16.7±5.5	8.9±3.2	6.8±2.7	11.4±3.4
Mn total	9.6±3.4	5.5±2.2	3.0±1.4	1.3±0.7	

these curves fall off exponentially. These features are reproduced by the DWBA calculations, which are shown in Fig. 7. The solid lines in Fig. 6 for the ^{59}Ni, ^{60}Ni, ^{61}Ni, ^{57}Co, and ^{56}Fe channels are least-squares fits to data points beyond the strong absorption region ($D>13.8$ fm). For the ^{62}Ni, ^{63}Ni, and ^{64}Ni channels, which have considerable smaller cross sections, the solid lines serve to guide the eye.

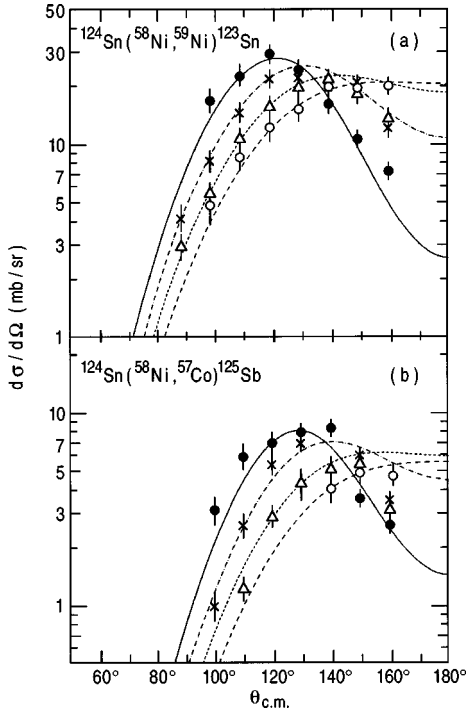

FIG. 5. DWBA calculations compared with the experimental data for (a) one-neutron pickup and (b) one-proton stripping at four energies for the system ^{58}Ni+^{124}Sn. The configurations for the outgoing channels taken into account in the calculations are ^{59}Ni(0.0,3/2$^-$)+^{123}Sn(0.150,1/2$^+$) and ^{57}Co(1.378,3/2$^-$) +^{125}Sb(0.700,1/2$^+$), respectively. Closed circle and solid line: $E_{c.m.}=160.6$ MeV, cross and dot-dashed line: $E_{c.m.}=157.0$ MeV, open triangle and dashed line: $E_{c.m.}=153.0$ MeV, open circle and long-dashed line: $E_{c.m.}=150.0$ MeV.

In semiclassical models it can be shown [20] that the ratio $P_{tr}/\sin(\theta_{c.m.}/2)$ depends exponentially on the distance of closest approach D via

$$\frac{P_{tr}}{\sin(\theta_{c.m.}/2)} \propto \exp(-2\alpha D), \tag{3}$$

where the exponential decay constant α is determined by the binding energy B of the donor (or acceptor) nucleus before (or after) the reaction, i.e.,

$$\alpha = \sqrt{\frac{2\mu B}{\hbar^2}}. \tag{4}$$

Here μ is the reduced mass of the transferred nucleon or nucleon cluster. Many systems have been analyzed with this formula [21–33]. The decay constants α observed for one-nucleon transfer reactions usually agree quite well with the values obtained from the semiclassical model. For two-nucleon transfer the observed decay constant agrees with the semiclassical model only when the incident energy is below the Coulomb barrier. At higher incident energies, the extracted decay constant obtained is usually smaller. While Wuosmaa *et al.* [21] explained this observation by considering diffractive rather than semiclassical scattering, Baba *et al.* [22] found that this can also be understood within the semiclassical models if the contributions from both the nuclear and the Coulomb branch of the classical deflection function are considered.

The decay constants derived from the experiments are given in Table III. For one-neutron pickup and one-proton stripping reactions the decay constants agree with the values derived from the binding energies. For two-neutron transfer reaction only 80% of the decay constant predicted by Eq. (4) is observed. For the three-neutron transfer a similar fraction (73%) of the expected decay constant is observed. For more

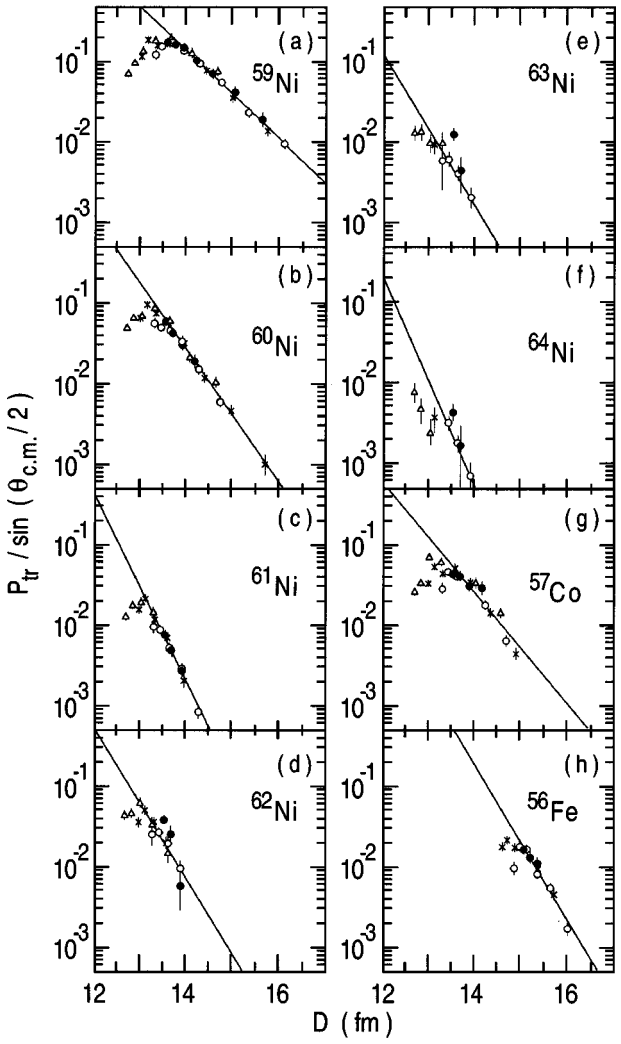

FIG. 6. $P_{tr}/\sin(\theta_{c.m.}/2)$ plotted versus D for one- to six-neutron pickup and one- to two-proton stripping channels in the system ^{58}Ni+^{124}Sn for four energies. See text for definitions of P_{tr} and D. Open triangle: $E_{c.m.}=160.6$ MeV, cross: $E_{c.m.}=157.0$ MeV, open circle: $E_{c.m.}=153.0$ MeV, closed circle: $E_{c.m.}=150.0$ MeV. The solid lines for channels ^{59}Ni, ^{60}Ni, ^{61}Ni, ^{57}Co, and ^{56}Fe are least-square fits to data points beyond the strong absorption region ($D>13.8$ fm). The lines for the ^{62}Ni, ^{63}Ni, and ^{64}Ni channels serve to guide the eye.

complex transfer reactions, the decay constants seem to saturate at $\alpha\sim1.5$ fm^{-1}, although, due to the small cross sections, the experimental uncertainties are quite large.

C. Energy dependence of multineutron transfer reactions

Angle- and energy-integrated cross sections are plotted in Fig. 8 as function of the number of transferred neutrons for the four incident energies. Similar to the results obtained in the system ^{58}Ni+^{100}Mo, the cross sections falloff exponentially as function of the number of transferred neutrons. The solid lines in Fig. 8 are least-squares fits to the data which give reduction factors for the cross sections of 4–5 per each transferred neutron. The energy dependence of the average reduction factor is given in Table IV, together with the results obtained for ^{58}Ni+^{100}Mo [4], ^{40}Ca+^{124}Sn [5], and for ^{112}Sn+^{120}Sn [34]. In the last system only one- to four-

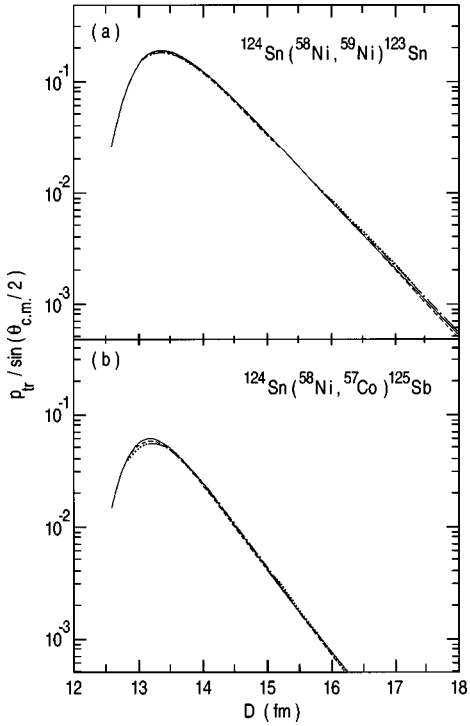

FIG. 7. $P_{tr}/\sin(\theta_{c.m.}/2)$ versus D plots from DWBA calculations at four energies for the system ^{58}Ni+^{124}Sn. (a) one-neutron pickup channel and (b) one-proton stripping channel. Solid line: $E_{c.m.}=160.6$ MeV, dashed line: $E_{c.m.}=157.0$ MeV, dotted line: $E_{c.m.}=153.0$ MeV, dot-dashed line: $E_{c.m.}=150.0$ MeV.

neutron transfer reactions have been observed. A smooth increase in the reduction factor is observed with decreasing energy. At energies around the Coulomb barrier all systems show values of about 4. This is near the value of 4–5 found in Ref. [35], where this reduction factor was obtained from a systematic study of one- and two-neutron transfer reactions induced by various projectiles.

We have applied the code GRAZING [6] to calculate the angle- and energy-integrated neutron pickup cross sections. The results at the highest energy ($E_{c.m.}=160.6$ MeV) are shown in Fig. 9 in comparison with the data. While the

TABLE III. Decay constants (in fm^{-1}) obtained from the experiments (α_{exp}), from the semiclassical model (α_{semi}) and DWBA calculations (α_{DWBA}) for the system ^{58}Ni+^{124}Sn, Don. and acc. denote what is calculated from donor or acceptor nucleus. See text for details.

Channel	α_{exp}	α_{semi} Don.	α_{semi} Acc.	α_{DWBA}
^{59}Ni	0.63±0.06	0.638	0.653	0.66
^{60}Ni	0.94±0.09	1.171	1.380	
^{61}Ni	1.33±0.16	1.813	1.971	
^{62}Ni	1.23±0.25			
^{63}Ni	1.26±0.25			
^{64}Ni	1.50±0.25			
^{57}Co	0.80±0.16	0.623	0.761	0.83
^{56}Fe	0.96±0.18	1.151	1.453	

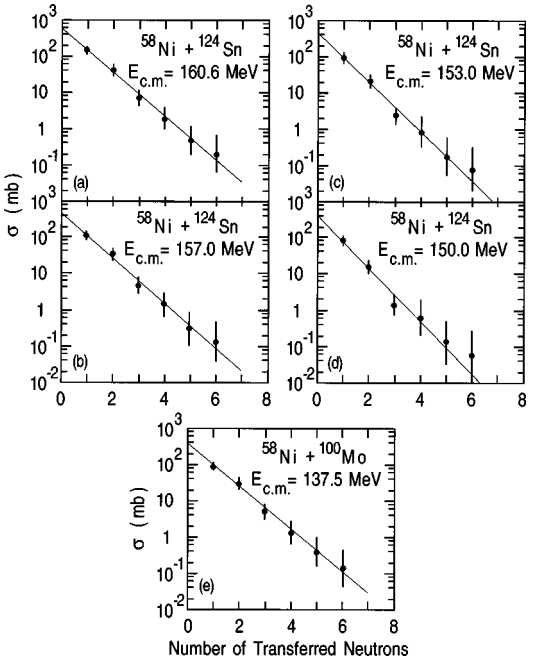

FIG. 8. Angle- and energy-integrated cross sections as a function of the number of transferred neutrons for the system ^{58}Ni $+^{124}$Sn at four incident energies, together with data for the system ^{100}Mo$+^{58}$Ni [4]. The solid lines are least-squares fits to the data. The reduction factors for each transferred neutron are given in Table IV.

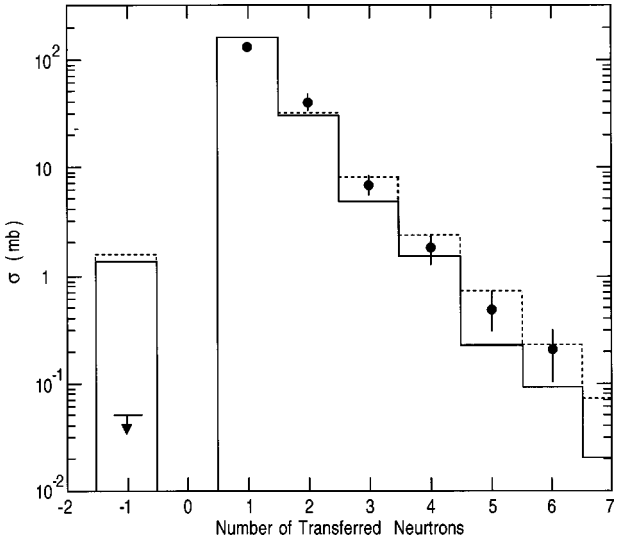

FIG. 9. Cross section calculations with the code Grazing in comparison with the experimental data for neutron transfer reactions in the system ^{58}Ni$+^{124}$Sn at $E_{\text{c.m.}}=160.6$ MeV. While the dashed line gives the results without neutron evaporation corrections, neutron evaporation is included in the solid line.

dashed lines give the results without neutron evaporation corrections, neutron evaporation is included in the solid line. The calculated average reduction factor is 4.46 (after evaporation correction) and 3.73 (without correction), close to the experimental value of 4.02. The calculation, however, overpredicts the one-neutron stripping cross section by one to two orders of magnitude. Because this code was designed to study reaction mechanisms above the Coulomb barrier, we have not applied it to the data taken at the three lower energies.

No significant enhancement of the cross section for pair transfer is seen in the energy-integrated cross sections. However, it is noticed that at all energies shown in Fig. 8 the one-pair (i.e., two-neutron) transfer cross section is always higher than the fitted average value, and that the three-neutron transfer cross section is always below the fitted average value.

Similar observations were made for ^{58}Ni$+^{100}$Mo [4], and in the study of ^{40}Ca$+^{124}$Sn [5], where the cross sections for the two-neutron pickup reaction are also higher than the interpolated value from the one-neutron and three-neutron cross sections, independent of how many protons were stripped (from one-proton to four-proton). The same trend is seen in the neutron-pickup cross sections for ^{48}Ca$+^{124}$Sn [7].

A possible reason for this behavior might be that the ground state Q value Q_{gg} for two-neutron transfer is positive and larger than the Q values for one-neutron and three-neutron transfer, and thus a larger region in excitation energy is accessible for the two-neutron transfer. The other possibility might be a slightly enhanced direct pair neutron transfer contribution in the reaction process. This possibility will be studied in the following paper [14].

D. Q value spectra

Q-value spectra for the one- to six-neutron pickup channels, measured at $\theta_{\text{lab}}=20°$ and $E_{\text{c.m.}}=153.0$ MeV, and integrated over the four charge states $q=23$–26 are presented in Fig. 10. As the number of transferred neutrons increases, the centroids of these distributions are seen to move to higher excitation energies, and the widths increase considerably. The same trend was observed for ^{58}Ni$+^{100}$Mo [4]. We shall now try to make a simple estimate of the centroid of the experimental Q-value distribution.

Within the simple Q-matching picture, the optimum Q value (without recoil correction) is given by $Q_{\text{opt}}=0$ (i.e., $E_{ex}\sim Q_{gg}$), while experimentally, more negative values are observed. Before a collision, the velocities of ^{124}Sn and ^{58}Ni in the center-of-mass system are denoted by V_2 and V_1, respectively, and the center-of-mass energy is $E_{\text{c.m.}}=(M_1$

TABLE IV. Reduction factor of the cross section per each transferred neutron, obtained from least-square fits to the cross sections. For comparison the data for the systems ^{58}Ni$+^{100}$Mo [4], ^{40}Ca$+^{124}$Sn [5], and ^{112}Sn$+^{120}$Sn [34] are also included.

$E_{\text{c.m.}}$(MeV) = 160.6	157.0	153.0	150.0	137.5 ^{58}Ni$+^{100}$Mo	127.9 ^{40}Ca$+^{124}$Sn	263-278 ^{112}Sn$+^{120}$Sn
4.02±.30	4.18±.36	4.79±.45	5.35±.57	3.88±.30	4.04	4.15

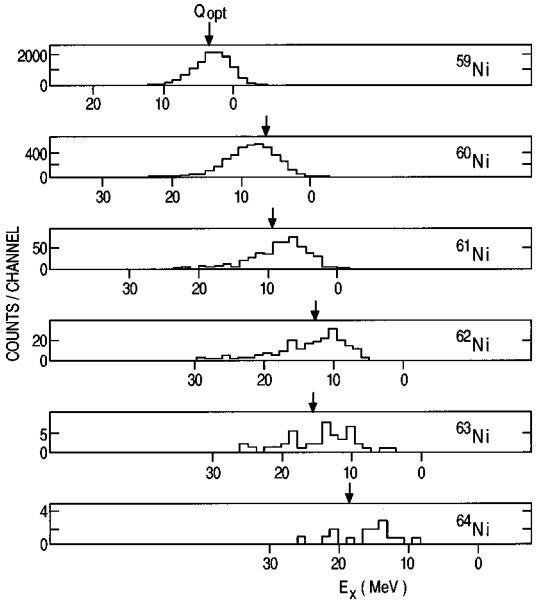

FIG. 10. Measured Q-value spectra for neutron pickup channels at $E_{\mathrm{c.m.}}=153.0$ MeV, $\theta_{\mathrm{lab}}=20°$, integrated over the charge states $q=23$–26. The solid arrows indicate the estimated Q_{opt}.

$+M_2)(M_2/M_1)V_2^2/2$. After the collision, X neutrons have been transferred from ^{124}Sn to ^{58}Ni, and the new velocities are denoted by V_2' and V_1', respectively. The center-of-mass energy is now $E'_{\mathrm{c.m.}}=(M_1+M_2)[(M_2-X)/(M_1+X)]V_2'^2/2$. If we assume that there is no energy exchange between $^{(124-X)}$Sn and the X neutrons, that is $V_2'=V_2$, then ^{58}Ni $+X$ neutrons will receive the momentum XV_2 from the transferred X neutrons. The associated Q value is called Q_{semi}, and it is given by

$$Q_{\mathrm{semi}}=-E_{\mathrm{c.m.}}\frac{(M_1+M_2)X}{M_2(M_1+X)}, \tag{5}$$

with $M_1=58$, and $M_2=124$.

Equation (5) is similar to that obtained by Mermaz *et al.* [36] for reactions at higher bombarding energies. In addition to the Q_{semi}, the ground state Q value Q_{gg} and recoil effect contribute to the total Q value. Anantaraman *et al.* considered the recoil effect in an estimation of optimum Q values for (^{16}O,C) reactions below the barrier [37]. For neutron transfer reactions the recoil contribution is

$$Q_{\mathrm{recoil}}=E_{\mathrm{c.m.}}\left(\frac{Z_f z_f}{Z_i z_i}\beta-1\right), \tag{6}$$

with $\beta=D_i/D_f$, where D_i and D_f are the distances between the projectile and target, and between the outgoing particle and the residual nucleus, respectively (see Ref. [37]). The total optimum Q value Q_{opt} is then given by

$$Q_{\mathrm{opt}}=Q_{gg}+Q_{\mathrm{semi}}+Q_{\mathrm{recoil}}. \tag{7}$$

The experimental Q_{exp} and the estimated Q_{opt} values are compared in Table V. The solid arrows in Fig. 10 indicate the positions of Q_{opt}. It is seen that Q_{opt} reproduces the average value of Q_{exp} reasonably well.

TABLE V. Experimental Q values Q_{exp} for neutron-pickup channels (at $E_{\mathrm{c.m.}}=153.0$ MeV, $\theta_{\mathrm{lab}}=20°$, and integrated over the charge states $q=23$–26) and estimated values Q_{opt} from a semiclassical model. See text for details.

Channel	Q_{semi} (MeV)	Q_{gg} (MeV)	Q_{recoil} (MeV)	Q_{opt} (MeV)	Q_{exp} (MeV)
^{59}Ni	-3.81	0.511	0.47	-2.9	-2.6
^{60}Ni	-7.49	5.95	0.87	-0.7	-2.5
^{61}Ni	-11.0	4.96	1.28	-4.8	-4.0
^{62}Ni	-14.5	9.39	1.66	-3.4	-3.9
^{63}Ni	-17.8	7.11	2.03	-8.8	-7.7
^{64}Ni	-21.1	10.29	2.38	-8.5	-6.0

IV. SUMMARY

We have measured angular distributions for elastic scattering and multinucleon transfer reactions in ^{58}Ni+^{124}Sn collisions with good particle identification at energies around the barrier. The four angular distributions for elastic and inelastic scattering can be well described by coupled-channels calculations. The angular distributions of one-nucleon transfer reactions are also well described by DWBA calculations using the same optical potential. The transfer probabilities for each transfer channel plotted as function of the distance of closest approach fall on a common curve. For one-neutron pickup and one-proton stripping reactions the decay constants agree with the values derived from the semiclassical model. For multinucleon reaction channels the decay constants are all smaller than the semiclassical model values, and seem to saturate at $\alpha\sim1.5$ fm^{-1}.

The cross sections for one- to six-neutron pickup reactions have been measured. The angle- and energy-integrated cross sections exhibit an exponential falloff with increasing number of transferred neutrons. The average reduction in cross section per each transferred neutron has been extracted and the energy dependence of the reduction factor has been determined. At the highest center-of-mass energy this average reduction agrees well with the predictions made with Winther's code GRAZING [6].

The centroids of the Q-value spectra for the one- to six-neutron pickup channels move towards higher excitation energies, and the widths increase considerably as the number of transferred neutrons increases. The detailed reaction mechanism for these multineutron transfer reactions, such as the sharing of excitation energies between the two reaction partners is not known. A comprehensive coupled-channels analysis of the data measured in this experiment as well as for other reaction channels in the system ^{58}Ni+^{124}Sn will be given in the following paper [14].

ACKNOWLEDGMENTS

We want to thank the crew of the ATLAS accelerator for providing the stable ^{124}Sn beams used in the experiments. We also thank Professor A. Winther for providing us with his code GRAZING. This work was support by the U.S. Department of Energy, Nuclear Physics Division, under Contract No. W-31-109-ENG-38.

[1] C. H. Dasso, G. Pollarolo, and A. Winther, Phys. Rev. Lett. **73**, 1907 (1994).
[2] C. H. Dasso, G. Pollarolo, and A. Winther, Phys. Rev. C **52**, 2264 (1995).
[3] J. Speer, W. von Oertzen, D. Schüll, M. Wilpert, H. G. Bohlen, B. Gebauer, B. Kohlmeyer, and F. Pühlhofer, Phys. Lett. B **259**, 422 (1991).
[4] C. L. Jiang, K. E. Rehm, J. Gehring, B. Glagola, W. Kutschera, M. Rhein, and A. H. Wuosmaa, Phys. Lett. B **337**, 59 (1994).
[5] L. Corradi *et al.*, Phys. Rev. C **54**, 201 (1996).
[6] A. Winther, Nucl. Phys. **A594**, 203 (1995); A. Winther, *ibid.* **A572**, 191 (1994); A. Winther (private communications).
[7] L. Corradi, A. M. Stefanini, J. H. He, S. Beghini, G. Montagnoli, F. Scarlassara, G. F. Segato, G. Pollarolo, and C. H. Dasso, Phys. Rev. C **56**, 1 (1997).
[8] W. E. Freeman, H. Ernst, D. F. Geesaman, W. Henning, T. J. Humanic, W. Kühn, G. Rosner, J. P. Schiffer, and B. Zeidman, Phys. Rev. Lett. **50**, 1563 (1983).
[9] K. T. Lesko, W. Henning, K. E. Rehm, G. Rosner, J. P. Schiffer, G. S. F. Stephans, and B. Zeidman, Phys. Rev. Lett. **55**, 803 (1985); K. T. Lesko, W. Henning, K. E. Rehm, G. Rosner, J. P. Schiffer, G. S. F. Stephans, and B. Zeidman, Phys. Rev. C **34**, 2155 (1986).
[10] R. R. Betts *et al.*, Phys. Rev. Lett. **59**, 978 (1987); C. N. Pass *et al.*, Nucl. Phys. **A499**, 173 (1989).
[11] W. Henning, F. L. H. Wolfs, J. P. Schiffer, and K. E. Rehm, Phys. Rev. Lett. **58**, 318 (1987).
[12] A. M. van den Berg, W. Henning, L. L. Lee, Jr., K. T. Lesko, K. E. Rehm, J. P. Schiffer, G. S. F. Stephans, and F. L. H. Wolfs, Phys. Rev. Lett. **56**, 572 (1986); A. M. van den Berg, W. Henning, L. L. Lee, Jr., K. T. Lesko, K. E. Rehm, J. P. Schiffer, G. S. F. Stephans, and F. L. H. Wolfs, Phys. Rev. C **37**, 178 (1988).
[13] F. L. H. Wolfs, W. Henning, K. E. Rehm, and J. P. Schiffer, Phys. Lett. B **196**, 113 (1987).
[14] H. Esbensen, C. L. Jiang, and K. E. Rehm, following paper, Phys. Rev. C **57**, 2401 (1998).
[15] K. E. Rehm and F. L. H. Wolfs, Nucl. Instrum. Methods Phys. Res. A **273**, 262 (1988).
[16] M. H. Macfarlane and S. C. Pieper, Argonne National Laboratory Report No. ANL-76-11 (Rev. 1), 1978 (unpublished).
[17] S. Raman, C. H. Malarkey, W. T. Milner, C. W. Nestor, Jr., and P. H. Stelson, At. Data Nucl. Data Tables **36**, 1 (1987).
[18] L. C. Vaz and J. M. Alexander, Phys. Rep. **69**, 373 (1981).
[19] K. E. Rehm, D. G. Kovar, W. Kutschera, M. Paul, G. Stephans, and J. L. Yntema, Phys. Rev. Lett. **51**, 1426 (1983).
[20] R. Bass, *Nuclear Reactions with Heavy Ions* (Springer, Berlin, 1980).
[21] A. H. Wuosmaa, K. E. Rehm, B. G. Glagola, Th. Happ, W. Kutschera, and F. L. H. Wolfs, Phys. Lett. B **255**, 316 (1991).
[22] C. V. K. Baba, V. M. Datar, K. E. G. Löbner, A. Navin, and F. J. Schindler, Phys. Lett. B **338**, 147 (1994).
[23] C. Y. Wu *et al.*, Phys. Rev. C **39**, 298 (1989).
[24] K. E. Rehm, B. G. Glagola, W. Kutschera, F. L. H. Wolfs, and A. H. Wuosmaa, Phys. Rev. C **47**, 2731 (1993).
[25] J. F. Liang, L. L. Lee, Jr., J. C. Mahon, and R. J. Vojtech, Phys. Rev. C **47**, 1342 (1993); **50**, 1550 (1994); R. B. Roberts, S. B. Gazes, J. E. Mason, M. Satteson, S. G. Teichmann, L. L. Lee, Jr., J. F. Liang, J. C. Mahon, and R. J. Vojtech, *ibid.* **47**, 1831 (1993).
[26] D. Tomasi *et al.*, Phys. Rev. C **48**, 2840 (1993).
[27] D. M. Herrick, F. L. H. Wolfs, D. C. Bryan, C. G. Freeman, K. L. Kurz, D. H. Mathews, P. A. A. Perera, and M. T. Zanni, Phys. Rev. C **52**, 744 (1995).
[28] M. Devlin, D. Cline, R. Ibbotson, M. W. Simon, and C. Y. Wu, Phys. Rev. C **53**, 2900 (1996).
[29] F. J. Schindler *et al.*, Nucl. Phys. **A603**, 77 (1996).
[30] D. Tomasi *et al.*, Phys. Rev. C **54**, 1282 (1996).
[31] S. Juutinen *et al.*, Phys. Lett. B **192**, 307 (1987).
[32] C. Y. Wu *et al.*, Phys. Rev. C **39**, 298 (1989).
[33] W. J. Kernan *et al.*, Nucl. Phys. **A524**, 344 (1991).
[34] W. von Oertzen, H. G. Bohlen, B. Gebauer, R. Künkel, F. Pühlhofer, and Schüll, Z. Phys. A **326**, 463 (1987).
[35] K. E. Rehm, C. Beck, A. van den Berg, D. G. Kovar, L. L. Lee, Jr., W. C. Ma, F. Videbaek, and T. F. Wang, Phys. Rev. C **42**, 2497 (1990).
[36] M. C. Mermaz *et al.*, Nucl. Phys. **A441**, 129 (1985).
[37] N. Anantaraman, K. Katori, and J.P. Schiffer, in *Symposium on Heavy-ion Transfer Reactions* (Argonne National Laboratory, Argonne, 1973), Vol. II, p. 413; a similar discussion can be found in Ref. [20].